



HAL
open science

Effect of Mn loading onto hydroxyapatite supported Mn catalysts for toluene removal: Contribution of PCA assisted ToF-SIMS

Dayan Chlala, Anne Constant, Nicolas Nuns, Jean-Marc Giraudon, Madona Labaki, Jean-Francois Lamonier

► To cite this version:

Dayan Chlala, Anne Constant, Nicolas Nuns, Jean-Marc Giraudon, Madona Labaki, et al.. Effect of Mn loading onto hydroxyapatite supported Mn catalysts for toluene removal: Contribution of PCA assisted ToF-SIMS. *Catalysis Today*, 2018, *Catalysis Today*, 307, pp.41-47. 10.1016/j.cattod.2017.04.018 . hal-03153470

HAL Id: hal-03153470

<https://hal.univ-lille.fr/hal-03153470v1>

Submitted on 1 Dec 2023

HAL is a multi-disciplinary open access archive for the deposit and dissemination of scientific research documents, whether they are published or not. The documents may come from teaching and research institutions in France or abroad, or from public or private research centers.

L'archive ouverte pluridisciplinaire **HAL**, est destinée au dépôt et à la diffusion de documents scientifiques de niveau recherche, publiés ou non, émanant des établissements d'enseignement et de recherche français ou étrangers, des laboratoires publics ou privés.

Effect of Mn loading onto hydroxyapatite supported Mn catalysts for toluene removal: Contribution of PCA assisted ToF-SIMS

D. Chlala^{1,2}, A. Griboval-Constant^{1,*}, N. Nuns¹, J.-M. Giraudon^{1,*},
M. Labaki², J.-F. Lamonier¹

¹ Univ. Lille, CNRS, Centrale Lille, ENSCL, Univ. Artois, UMR 8181 - UCCS - Unité de Catalyse et Chimie du Solide, F-59000 Lille, France

² Lebanese University, Laboratory of Physical Chemistry of Materials (LCPM)/PR2N, Faculty of Sciences, Fanar, BP 90656 Jdeidet El Metn, Lebanon

**Corresponding authors*

E-mail : anne.griboval@univ-lille1.fr, jean-marc.giraudon@univ-lille1.fr

Keywords: Chemometrics, PCA, ToF-SIMS, catalysis, toluene, total oxidation.

Abstract:

A series of hydroxyapatite (Hap; of ideal formula: $\text{Ca}_{10}(\text{PO}_4)_6(\text{OH})_2$) supported MnO_x materials (Mn_xHap ; $x = \text{Mn wt.}\%$: 2.5, 5.0, 10, 20, and 30 based on MnO_2) has been tested in toluene total oxidation (800 ppmv in dry air) at 220°C for 40h. It was shown that the fresh catalysts can be ranked as follow by decreasing activity: $\text{Mn5Hap} > \text{Mn2.5Hap} > \text{Mn10Hap} > \text{Mn20Hap} > \text{Mn30Hap}$ and that Mn10Hap exhibited the best resistance to deactivation. Investigation of the surface state of the fresh and used catalysts has been performed using X-ray photoelectron spectroscopy (XPS) and principal component analysis (PCA) assisted static time-of-flight secondary-ion mass spectrometry (ToF-SIMS). Based on the XPS results a Mn speciation scheme can be proposed: initial incorporation of Mn^{2+} into Hap (2.5 wt% Mn) followed by additional well dispersed oxidized manganese species on Hap (5-10 wt% Mn) to end up with the formation $\text{Mn}_2\text{O}_3/\varepsilon\text{-MnO}_2$ particles detected by XRD (20-30 wt% Mn). Principal components analysis (PCA) has been applied to the (+) ToF-SIMS spectra taking into account of all the detected significant manganese containing secondary ions. PC1 (75% of the variance) discriminates well the fresh and used samples in a similar way and was related to the surface manganese content. The resulting volcano plot obtained by plotting PC2 (12% of the variance) as a function of the resistance to deactivation discriminates the catalysts in the same way as depicted in the PC2 score plot. Consequently, also taking into account of the PC2 loading plot it was suggested that a redispersion of $\text{Mn}^{n+}/\text{Ca}^{2+}$ takes place with time on stream preferentially for Mn_xHap ($x = 5\text{-}10 \text{ wt}\%$) improving their catalyst stability.

1. Introduction

Hydroxyapatite (Hap) based materials have attracted much interest for use in a variety of applications since they are safe, non-toxic, inexpensive and readily available in the natural environment [1]. Furthermore, these materials present a high chemical and thermal stability and a weak solubility in water. It is also of importance in many industrial applications, such as catalysis, ion exchange, and metal removal [2-5]. However, few studies deal with the dispersion of an active phase such as transition metal oxides on hydroxyapatite [6,7]. Supported MnO_x catalyst may provide a viable prospect for total oxidation of volatile organic compounds (VOCs) as MnO_x catalysts exhibit an easy redox cycling ability, have long-lifetime, low cost and have biocompatibility properties. With that respect Hap supported oxidized Mn (Mn: 10 wt%) catalysts have been recently investigated for total oxidation of toluene and the effect of the counter-anion of the Mn(II) precursor has been particularly studied [8]. The best catalytic performances have been associated with the nitrate Mn(II) precursor. The Mn oxidized species well dispersed on Ca^{2+} enriched apatite were responsible for a good toluene conversion. By opposition the calcination performed with the acetate Mn precursor resulted in a lower Mn dispersion responsible for a lower activity [8].

Another important question to address in the follow-up to this previous work is the effect of Mn loading by the highlight of possible surface-reactivity relationship. Efficient complementary tools for surface investigation can be X-ray photoelectron spectroscopy (XPS) and time-of-flight secondary-ion mass spectrometry (ToF-SIMS). Indeed, XPS which has a depth of detection of about 10 nm can give an average information considering the average state of Mn while ToF-SIMS due to its high mass resolution and sensitivity can provide molecular information in the outermost layers of the material (1-3nm) [9]. Such ToF-SIMS/ XPS combination has been successfully implemented to elucidate mechanism of catalyst deactivation in oxidation of chlorinated VOCs as well as the beneficial role of water in the performances of a post-plasma catalytic process [10-11]. However, the great number of secondary ions in the ToF-SIMS spectra makes direct data interpretation impossible. The application of a Multivariate analysis (MVA) is, therefore, necessary. Among them the principal component analysis (PCA) [9,12-15] is of considerable interest due to its successfully application in the processing of ToF-SIMS data of organic and biological materials [16-21]. In the field of heterogeneous catalysis a few studies have been carried out using chemometrics to better interpret the catalytic performances in terms of chemical and physical properties of the catalysts [22-28]. PCA has been previously applied to evaluate the influence of different parameters such as temperature, pressure, Gas Hourly Space Velocity (GHSV), H_2/CO ratio on the catalytic performances of rhodium promoted catalyst supported on silica for carbon monoxide hydrogenation [26]. J.E. Hensley *et al.* have shown that PCA is an effective tool for structure-reactivity correlation. Based on XPS data, PCA allows to clarify the role of surface carbide species, coke and oxidation for the deactivation of potassium-promoted cobalt molybdenum sulfide for the production of mixed alcohols synthesis [24]. PCA carried out to study the relationships between catalytic and physicochemical properties of Co_3O_4 supported on alumina with different loadings for methane combustion by Q. Wang *et al.* highlights the significance of Co species and the redox cycle [25].

In the present work, a series of hydroxyapatite supported MnO_x catalysts (Mn wt. %: 2.5, 5.0, 10, 20, and 30) has been prepared by wet impregnation using manganese(II) nitrate as precursor in order to investigate the effect of Mn loading on the catalytic performances in the total oxidation of toluene. For this purpose, the fresh and used catalysts have been studied by PCA assisted ToF-SIMS and XPS in order to find possible surface-reactivity relationships.

2. Materials and Methods

2.1. Synthesis of the catalysts

The hydroxyapatite supported manganese materials were prepared using the wet impregnation method. Samples loaded with 2.5, 5, 10, 20 and 30 wt.% of manganese (calculated using MnO₂ as the basis) were synthesized using Mn(NO₃)₂·4H₂O (Sigma Aldrich, purity: 97%) as the metal precursor. The support material, Hap synthesized according to previous procedure [8], was calcined at 400°C for 4 h prior to impregnation. The sample was subsequently dried at 80°C for 20 h and then cooled and ground to ensure a homogeneous particle distribution. The sample was then heated to 400°C at a heating rate of 2°C/min and was calcined at that temperature for 4h. The materials were labelled MnxHap where x stands for the Mn weight percentage.

2.2. Catalytic tests

Catalytic oxidation runs for abatement of toluene were performed in a continuous flow fixed bed Pyrex micro-reactor at atmospheric pressure. The reactive gas mixture was 800 ppmv of toluene diluted in air (100 mL/min) at a fixed GHSV of 30000 mL/(g.h). The flow rate was adjusted and controlled with digital flowmeter (MFC Mass Flow Controller). The micro reactor was placed in an electrical furnace which provides the required temperature for catalytic reaction. The catalysts were pretreated 2 h at 300 °C (10 °C/min) in flowing air (75 mL/min) before to be cooled at 220 °C (10°C/min). After temperature stabilization, a test of duration in 800 ppmv of toluene diluted in air (100 mL/min) was carried out for 40h. The catalysts were finally allowed to cool down to 20°C in static reactive atmosphere. The catalysts were labelled MnxHap-ATS where ATS means after test stabilization.

The concentrations of the gaseous species in inlet and outlet gas streams were analyzed online by Gas Chromatography (7860A Agilent Gas Chromatograph) equipped with a Thermal Conductivity Detector (TCD) and Flame Ionization Detector (FID) with two columns: Restek Shin Carbon ST/Silco HP NOC 80/100 micropacked, to separate permanent gases (Air, CO and CO₂) and a capillary column Cp-Wax 52 CB25 m, Ø = 0.25 mm, to separate hydrocarbons and aromatic compounds.

Toluene conversion (C_t), CO yield and rate of toluene conversion r, expressed in mole of reacted toluene per mole of manganese and per hour, were calculated as follows:

$$C_t(\%) = \frac{[\text{toluene}]_{\text{in}} - [\text{toluene}]_{\text{out}}}{[\text{toluene}]_{\text{in}}} \times 100$$

$$Y_{\text{CO}}(\%) = \frac{[\text{CO}]}{7[\text{toluene}]_{\text{in}}} \times 100$$

$$r = \frac{F \times C_t}{n_{\text{Mn}}}$$

Where [toluene]_{in} and [toluene]_{out} were toluene inlet and outlet concentrations, F was the flow rate (mol/h) of toluene and n_{Mn} was the molar amount of manganese.

2.3. XPS measurements

Spectroscopy XPS experiments were performed using an AXIS Ultra DLD Kratos spectrometer equipped with a monochromatised aluminum source (Al K_α = 1486.7 eV) and charge compensation gun. The binding energies were referenced to the C 1s core level at 285 eV. The atomic compositions were estimated from the Ca 2p, P 2p, C 1s, O 1s and Mn 2p core shell levels. The average oxidation state (AOS) of Mn was determined from the energy separation of the 2 peaks present in the Mn 3s core shell level (see below) with an uncertainty of ± 0.2.

2.4. ToF-SIMS

Positive and negative ToF-SIMS measurements were performed with a TOF.SIMS5 spectrometer (ION-TOF GmbH Germany) equipped with a bismuth liquid metal ion gun (LMIG). The tableted samples were bombarded with pulsed Bi₃⁺ primary ion beam (25 keV, 0.25 pA) rastered over a 500×500µm² surface area. With a data acquisition of 100 s, the total fluence does not amount up to 10¹² ions/cm² ensuring static conditions. Charge effects were

compensated by means of a 20 eV pulsed electron flood gun. In these experiments, the mass resolution ($m/\Delta m$) was about 3200 at $m/z = 175$ for Ca_2PO_4^+ . The secondary ions were identified by their exact mass, coupled with the appropriate intensities for the expected isotope pattern.

2.5. Principal Component Analysis

PCA was performed on a data set consisting of 20 non-saturated containing Mn secondary ions in positive polarity. These secondary ions were identified in bold character in **Table 1** which contained all the significant positive secondary ions amounting to 41. For this purpose, a PLS_Toolbox_794 (Eigenvector Research, Manson, Washington, USA) was run under MATLAB version 7.11.0 (R2010b) (The MathWorks, Natick, Massachusetts, USA). A pre-treatment procedure was performed before PCA analysis: (i) the peak intensities were first normalized with respect to total intensity of the selected ions. The result of the data normalization was a [10 x 20] matrix where the rows (10) were the fresh and used catalysts and the columns (20) were the variables, namely the normalized intensity of the Mn selected ions; (ii) auto-scaling was then performed in order to give equal significance to each m/z ion in the spectrum. After the pre-treatment procedure, the data were analyzed by PCA.

Table 1
List of ToF-SIMS positive selected ion-fragments.

| $\text{Ca}_x\text{O}_y\text{H}_w^+$ | $\text{Mn}_x\text{O}_y\text{H}_w^+$ | $\text{PMn}_x\text{O}_y\text{H}_w^+$ | $\text{Ca}_x\text{Mn}_y\text{O}_z\text{H}_w^+$ | $\text{Ca}_x\text{Mn}_y\text{P}_z\text{O}_t\text{H}_w^+$ |
|---|--|---|---|---|
| Ca ⁺ | Mn ⁺ | P ⁺ | CaMnO⁺ (1) | CaPO ₃ ⁺ |
| CaH ⁺ | MnO⁺ (11) | PMn₂O₃H⁺ (14) | CaMnO₂⁺ (2) | CaPO ₃ ⁺ |
| CaO ⁺ | Mn₂O₂⁺ (12) | | CaMnO₂H⁺ (3) | Ca ₂ PO ₃ ⁺ |
| CaOH ⁺ | Mn₂O₂H⁺ (13) | | Ca₂MnO₂⁺ (4) | Ca ₂ PO ₄ ⁺ |
| Ca ₂ O ⁺ | Mn₃O₃⁺ (15) | | Ca₂MnO₃⁺ (5) | Ca ₃ P ₂ O ₃ H ⁺ |
| Ca ₂ O ₂ ⁺ | Mn₃O₃H⁺ (16) | | Ca₂MnO₃H⁺ (6) | CaMn₂PO₄H⁺ (17) |
| Ca ₂ O ₂ H ⁺ | | | CaMn₂O₃⁺ (7) | CaMn₂PO₅⁺ (18) |
| Ca ₂ O ₃ ⁺ | | | CaMn₂O₃H⁺ (8) | Ca ₄ P ₂ O ₄ H ⁺ |
| Ca ₂ O ₃ H ⁺ | | | CaMn₃O₄⁺ (9) | Ca₂Mn₂PO₃H⁺ (19) |
| CO ₂ Ca ₂ ⁺ | | | Ca₂Mn₂O₄⁺ (10) | Ca₂Mn₂PO₆⁺ (20) |
| ClO ₂ Ca ₂ ⁺ | | | | Ca ₅ P ₂ O ₃ H ⁺ |
| | | | | Ca ₆ P ₂ O ₄ H ₂ ⁺ |

The number inside the brackets design the number of the variables in the matrix.

3. Results and discussion

3.1. Catalytic results

The Mn_xHap catalysts have been tested in dry air containing 800ppmv of toluene at atmospheric pressure and isothermal conditions (220°C) at a fixed GHSV of 30000mL/(g.h). **Fig.1** shows the evolution in toluene conversion with time-on-stream over the Hap supported Mn based catalysts. The rates of toluene removal expressed per mole of manganese have been reported in **Table 2**. The fresh catalysts can be ranked by decreasing activity as follows: Mn5Hap > Mn2.5Hap > Mn10Hap > Mn20Hap > Mn30Hap. It is observed a decrease in toluene conversion with time on steam for all catalysts but to different extents. To quantify the resistance against deactivation an activity coefficient **a₂₂₀**, was defined as the ratio between the toluene conversion after 40 h reaction to that at initial time [29]. Plot of **a₂₂₀** against Mn content given in **Fig.2a** shows a volcano plot whose position of the maximum corresponds to the most resistant catalyst towards deactivation, namely Mn10Hap. The ranking of the used catalysts by decreasing activity (cf. **Table 2**) now becomes: Mn5Hap-ATS ≈ Mn10Hap-ATS ≈ Mn2.5Hap-ATS > Mn20Hap-ATS >> Mn30Hap-ATS.

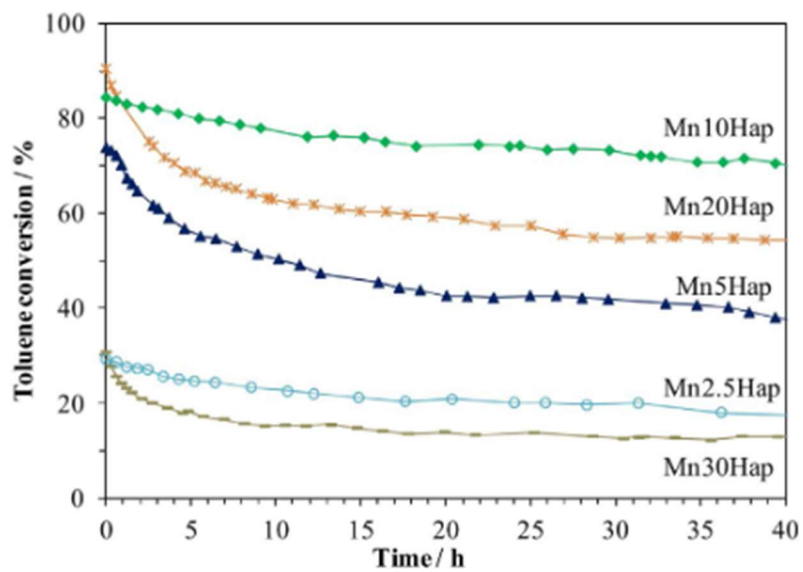


Fig. 1. Conversion of toluene as a function of time on stream over Mn_xHap catalysts.

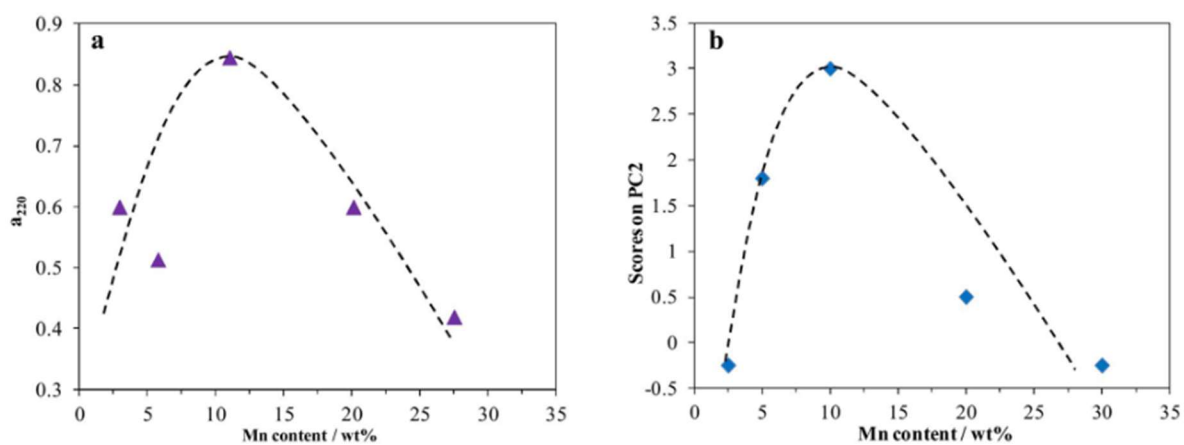


Fig. 2: a: Evolution of a_{220} as a function of Mn (wt%) content ; b: PC2 score as a function of Mn (wt%) content.

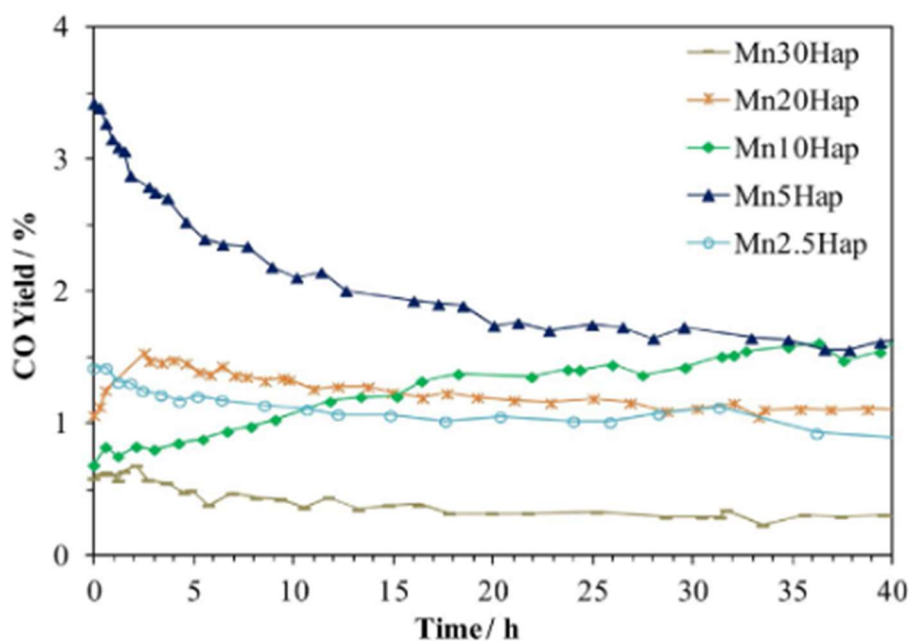


Fig. 3: CO yield as a function of time on stream over Mn_xHap catalysts.

Table 2
Toluene conversion and Toluene removal rate.

| Catalyst | $r/(\text{mol}_{\text{Tol}}/\text{h } n_{\text{Mn}})^{\text{a}}$ | Toluene conversion/% |
|--------------|--|----------------------|
| Mn2.5Hap | 0.5348 | 29 |
| Mn5Hap | 0.6942 | 74 |
| Mn10Hap | 0.4123 | 84 |
| Mn20Hap | 0.2420 | 90 |
| Mn30Hap | 0.0609 | 31 |
| Mn2.5Hap-ATS | 0.3320 | 18 |
| Mn5Hap-ATS | 0.3565 | 38 |
| Mn10Hap-ATS | 0.3485 | 71 |
| Mn20Hap-ATS | 0.1452 | 54 |
| Mn30Hap-ATS | 0.0255 | 13 |

^a Determined at 220 °C.

Along with CO₂, which is the main product of oxidation some amount of CO has also been detected. **Fig.3** displays CO yield as a function of time on stream for the different catalysts. The initial CO yield was the highest for Mn5Hap (3.4%) to decrease with time to reach 1.6% after 40h. Conversely the CO yield increases in the course of the reaction for Mn10Hap from 0.7 to 1.6% while it keeps rather stable with time regarding the remaining catalysts. Additionally, benzene and benzaldehyde were detected as gaseous by-products with concentrations ranging from 1.0-4.0 and 0.5-3.5 ppmv, respectively. It is to be noted that carbon balances are equal to or higher than 97%.

3.2. XPS results

XPS analysis has been performed to provide surface information regarding the effect of manganese loading on the Mn AOS and Mn dispersion. Mn AOS has been determined from the energy separation of two peaks which appear in the global envelope of the Mn 3s core level as

shown in **Fig. 4** and the relevant data as well as XPS compositions of the catalysts are reported in **Table 3**. The appearance of two peaks is due to the coupling of non-ionized 3s electron with 3d valence-band electrons. Interestingly the magnitude of the peak splitting ΔE is recognized to be a diagnostic of Mn AOS as ΔE decreases with the increase of Mn AOS. Some linear relationships between ΔE and Mn AOS have been reported in the literature and the one reported by Galakhov *et al.* [30] has been used in that work. Overall, for fresh samples, the Mn AOS increases from 1.7 to 3.7 with increased Mn content. The low Mn AOS of 1.7 in Mn2.5Hap, close to +2, can be explained by the diffusion of Mn as Mn^{2+} into the outermost layers of hydroxyapatite support, most likely, by exchange with Ca^{2+} surface sites.

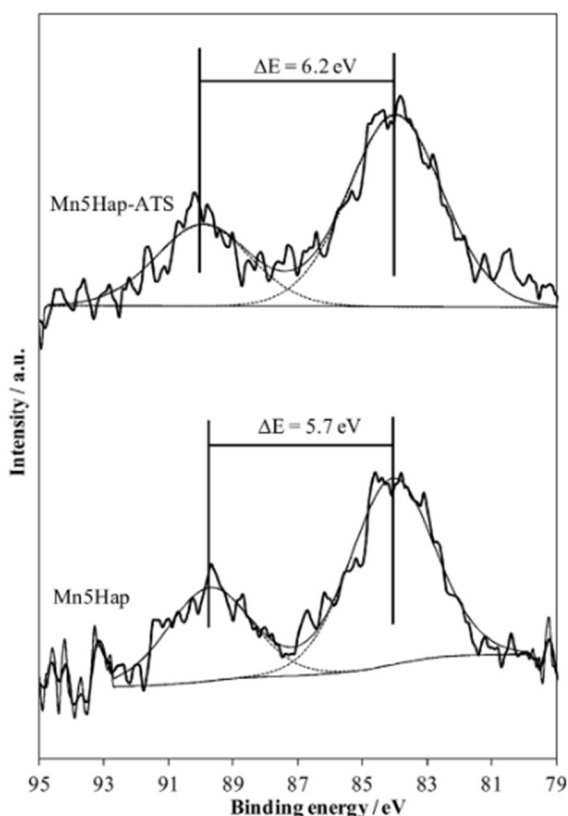


Fig. 4: Simulation of the XPS Mn 3s core level spectra of fresh and used Mn5Hap catalysts.

This is supported by the fact that the outermost layer of the bare Hap is enriched in Ca^{2+} as shown by LEIS [31] and that Mn^{2+} ion readily substitutes for Ca^{2+} in Hap [32]. The diffusion of Mn into the support during calcination therefore seems to be unavoidable despite the dispersion of Mn on Hap by wet impregnation. For medium Mn content (5-10 wt%) additional Mn can interact with the porous Hap surface to give well dispersed Mn oxide clusters with an Mn AOS of about 2.6 in accordance with the low temperature of calcination at 400°C and the oxidizing nature of the NO_3^- counter-anion of the Mn precursor. Finally, at higher Mn contents (20-30 wt%) nucleation and growth of manganese oxide particles with higher Mn valence (Mn AOS \approx 3.4-3.7) are expected to occur. This is consistent with the detection by X-ray diffraction (not shown in this study) of $\epsilon\text{-MnO}_2$ and $\epsilon\text{-MnO}_2/\text{Mn}_2\text{O}_3$ phases present in the Mn20Hap and Mn30Hap samples, respectively. **Fig.5a** shows a logarithmic evolution of the XPS atomic ratio $\text{Mn}/(\text{Ca} + \text{P})$ as a function of Mn loading both for fresh and spent Mn-Hap samples in agreement with a relative loss of Mn manganese dispersion with increasing Mn loading. Interestingly the higher position of the trace belonging to the used catalysts, due to higher $\text{Mn}/(\text{Ca} + \text{P})$ atomic ratio, might suggest a Mn surface in the depth probed by XPS. It should be noted that the Mn

AOS does not differ before and after catalysis for 10-20 wt% Mn loadings but clearly decreases for 5 wt% as shown in Fig.4 and 30 wt% Mn loadings (**Table 3**) due to toluene acting as reductant in accordance with a redox mechanism.

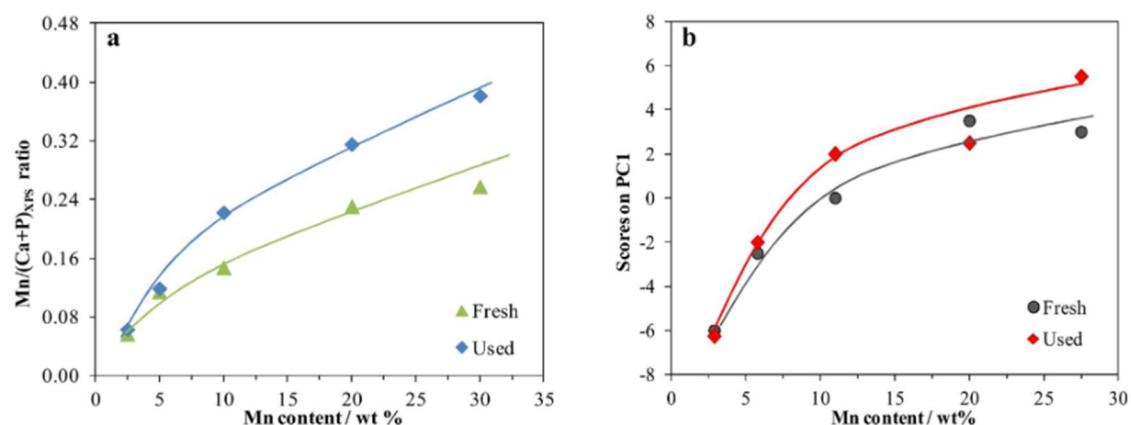


Fig. 5: a: Evolution of the surface atomic ratio Mn/(Ca + P) as a function of Mn loading ;
b: PC1 score as a function of Mn loading.

Table 3

XPS compositions of the fresh and used catalysts (in at%) and Mn AOS.

| Solids | Ca 2p | P 2p | O 1 s | C 1 s | Mn 2p | Mn AOS |
|--------------|-------|-------|-------|-------|-------|--------|
| Mn2.5Hap | 14.79 | 9.91 | 46.12 | 27.76 | 1.41 | 1.7 |
| Mn5Hap | 15.07 | 10.14 | 48.63 | 23.27 | 2.89 | 2.6 |
| Mn10Hap | 9.74 | 6.77 | 37.13 | 43.92 | 2.44 | 2.6 |
| Mn20Hap | 15.54 | 11.17 | 52.47 | 14.65 | 6.16 | 3.4 |
| Mn30Hap | 10.55 | 5.36 | 51.45 | 24.33 | 8.31 | 3.7 |
| Mn2.5Hap-ATS | 10.93 | 7.22 | 35.60 | 45.10 | 1.15 | 1.5 |
| Mn5Hap-ATS | 10.91 | 7.26 | 37.67 | 41.99 | 2.16 | 2.0 |
| Mn10Hap-ATS | 7.76 | 5.63 | 32.83 | 50.82 | 2.97 | 2.5 |
| Mn20Hap-ATS | 10.16 | 7.29 | 43.64 | 33.39 | 5.51 | 3.4 |
| Mn30Hap-ATS | 11.23 | 5.89 | 46.36 | 29.99 | 6.53 | 3.0 |

3.3. ToF-SIMS results

Regarding the Hap support, investigation of the (-) mass spectra of the investigated samples reveals the following peaks: O⁻, OH⁻, P⁻, O₂⁻, PO⁻, PO₂⁻, and PO₃⁻. The fragment ions of the PO₄³⁻ anion such as P⁻ (m/z = 30.97), PO⁻ (m/z = 46.97), PO₂⁻ (m/z = 62.96), and PO₃⁻ (m/z = 78.96) are clearly observed. The characteristic peaks shown in the (+) spectra include (ion, m/z value): Ca⁺, 39.96; CaO⁺, 55.96; CaOH⁺, 56.96 and Ca₂O⁺, 95.92. Some impurities are also detected such as Na⁺, Mg⁺, K⁺, and hydrocarbons. Several fragment ions were found to be derived from the Ca₁₀(PO₄)₆(OH)₂ support (ion, m/z value) such as Ca₂PO₃⁺, 158.88; Ca₂PO₄⁺, 174.88; Ca₃P₂O₃H⁺, 230.82; Ca₄P₂O₄H⁺, 286.78; Ca₅P₂O₅H⁺, 342.74; Ca₆P₃O₄H₂⁺, 398.69. Subtraction of the hydroxyl ion OH⁻ from Ca₅(PO₄)₃OH affords the ion Ca₅(PO₄)₃⁺ detected at m/z = 484.67.

The ToF-SIMS (-) spectra of the Hap supported Mn samples exhibit as the most characteristic intense Mn ions MnO₂H⁻, MnO₃⁻ and MnO₃H⁻ in the m/z 2-150 range. Additionally, the NO⁻, 30.00; NO₂⁻, 45.99 and NO₃⁻, 61.99 ions are clearly observed on the fresh Mn_xHap samples and

attest of the presence of residual nitrate after calcination.

All investigated ToF-SIMS (+) spectra evidence 10 secondary ions both containing Ca and Mn ions of general formula $\text{Ca}_v\text{Mn}_y\text{O}_z\text{H}_w^+$ ($v = 1,2$; $y = 1-3$; $z = 1-4$; $w = 0, 1$; labelled (1) to (10) in **Table 1**) among the overall Mn containing ions. As an example, **Fig.6** shows characteristic secondary ions in the 182-189 m/z range assigned to the Ca_2MnO_3 isotopic pattern.

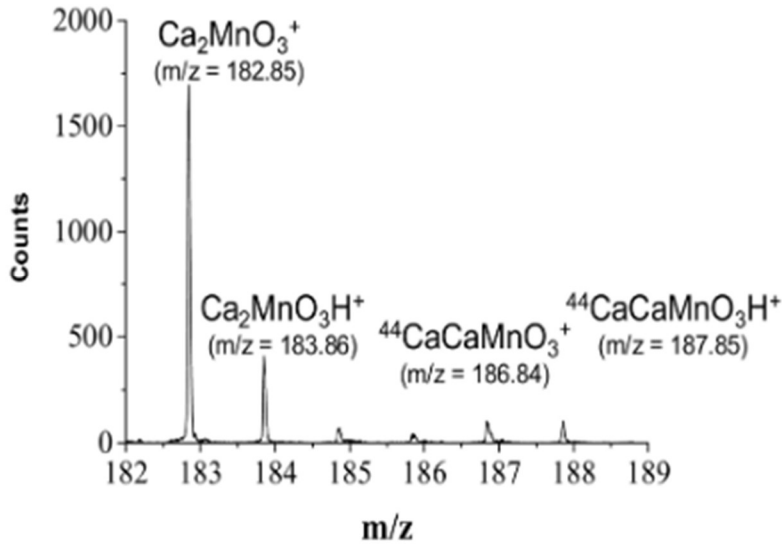


Fig. 6: ToF-SIMS (+) spectrum in the m/z 182-189 range collected from the Mn10Hap sample.

It is worth mentioning that the relative contribution of such secondary ions given in **Table 4** increases logarithmically as shown in **Fig.7** with Mn content in line with the detection of MnO_x particles at high Mn content.

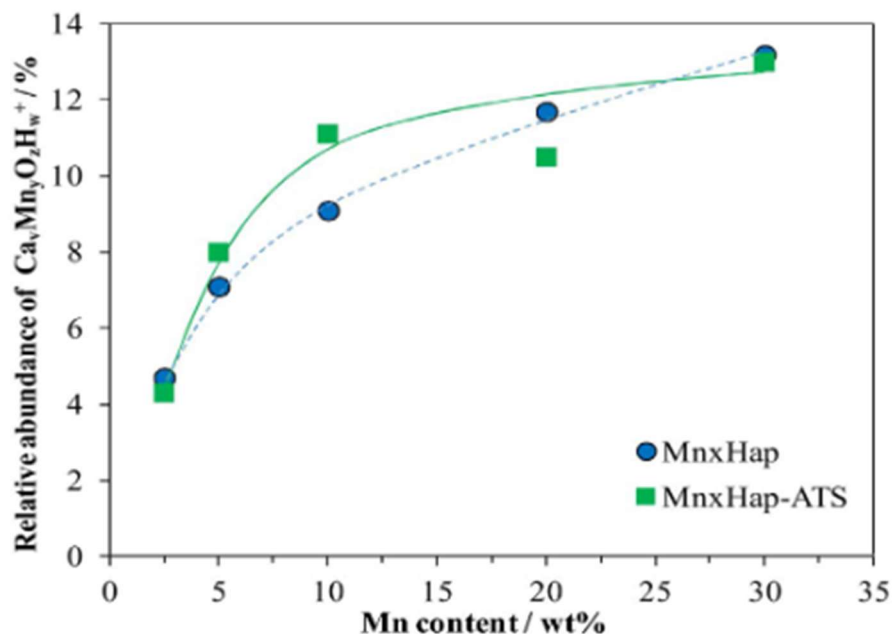


Fig. 7: Relative abundance of $\text{Ca}_v\text{Mn}_y\text{O}_z\text{H}_w^+$ secondary ions as a function of Mn content.

By contrast only one Mn-P related ion, namely $\text{PMn}_2\text{O}_3\text{H}^+$ (labelled (14) in **Table 1**) is observed. Furthermore, four $\text{CaMn}_2\text{PO}_4\text{H}^+$, $\text{CaMn}_2\text{PO}_5^+$, $\text{Ca}_2\text{Mn}_2\text{PO}_5\text{H}^+$ and $\text{Ca}_2\text{Mn}_2\text{PO}_6^+$ (labelled (17)-(20) in **Table 1**). Hence $\text{Ca}_v\text{Mn}_y\text{O}_z\text{H}_w^+$ (v, y, z

0) ions strongly contribute to the m/z signals of the spectra in comparison with $P_xMn_yO_zH_w^+$ (x, y, z # 0) indicating that manganese preferentially interacts with calcium than phosphorus. These observations are in accordance with previous works showing that the synthesis of hydroxyapatite using a reflux method allows to get an enriched Ca^{2+} surface as observed by LEIS [31] which is believed to promote a better Ca-O-Mn interaction. It should also be noted the observance of secondary ions such as $CaCO_3^+$ (m/z = 99.95) and $Ca_2HCO_3^+$ (m/z = 140.92) showing interaction of Ca^{2+} with carbonates.

3.4. Principal Component Analysis (PCA)

It is found that two PC account for about 87% of the data variance as seen in **Table 4**.

Table 4

Percentage of the variance captured by the PCA model for the system.

| Principal component number | Eigenvalue of Cov(X) | % Variance captured this PC | % Variance captured total |
|----------------------------|----------------------|-----------------------------|---------------------------|
| 1 | 15.700 | 74.55 | 74.55 |
| 2 | 2.550 | 12.15 | 86.69 |
| 3 | 1.350 | 6.43 | 93.12 |
| 4 | 0.800 | 3.81 | 96.93 |
| 5 | 0.496 | 2.36 | 99.30 |
| 6 | 0.103 | 0.49 | 99.79 |
| 7 | 0.021 | 0.10 | 99.89 |
| 8 | 0.016 | 0.08 | 99.96 |
| 9 | 0.008 | 0.04 | 100.00 |

The results are presented in a PC1-PC2 plot given in **Fig.8**. PC1 variability accounts for 75 % of total variance of the data set.

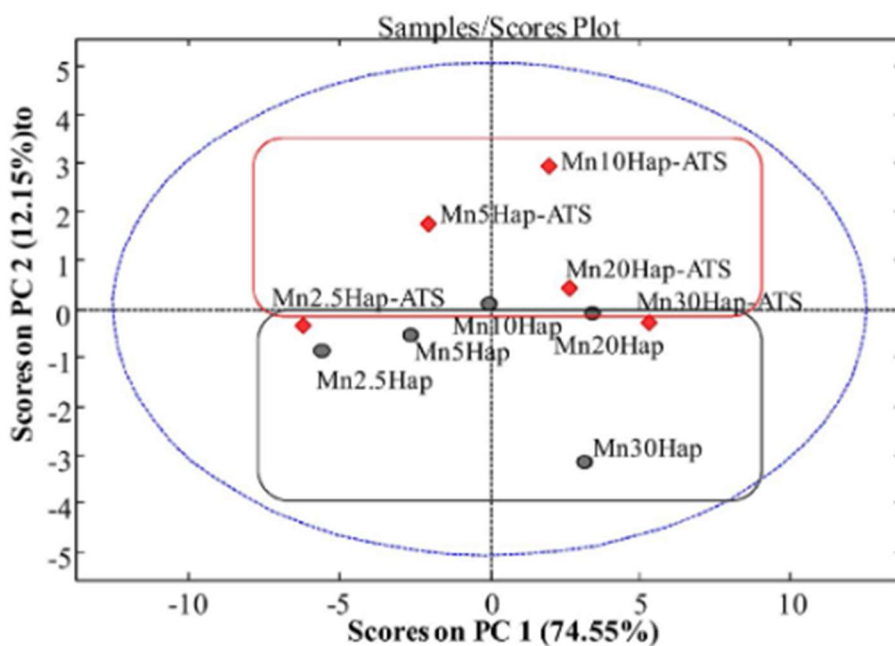


Fig. 8: PC1-PC2 score plot of the selected ToF-SIMS data.

Interestingly PC1 increases with Mn content up to 20 wt% with scores increasing from -5 to +4. Plot of PC1 score as a function of Mn content displayed in **Fig.5b** shows a logarithmically increase in a similar way to that previously noticed when plotting Mn/(Ca+P) ratio against Mn wt%. Hence PC1 provides information regarding manganese amount dispersed on the hydroxyapatite surface. Additionally, PC1 clearly enables to separate most of the used catalysts in a similar way than the fresh ones. As a consequence, similar conclusions hold for the used catalysts. Conversely it is found a clear discrimination among the fresh and used catalysts when considering the score plot of PC2 in **Fig.8**. Indeed, the PC2 splits the samples in two groups on both sides of PC2 score equal to 0. The used catalysts have globally a positive score while the fresh catalysts exhibit a negative one. Consequently, PC2 is mainly related to the manner according to which the reactive gaseous mixture affects the outermost layers of the samples. Additionally, it is observed in **Fig.2b** a volcano plot when plotting PC2 scores as a function of Mn loading for the used catalysts with the best PC2 score obtained for Mn10Hap. Based on the similarities with the previous volcano plot representing the coefficient factor a_{220} as a function of Mn loading (**Fig.2a**) it follows that PC2 is related to the extent of catalyst deactivation. Consequently, it is strongly suggested that a re-dispersion occurs during the first hours of the test on Mn x Hap catalysts ($x = 5-10$ wt%) implying significant changes in Ca-O-Mn interaction consistent with the higher loadings relative to the 2 variables CaOMn^+ and $\text{Ca}_2\text{MnO}_2^+$ m/z signals as shown in **Fig.9**.

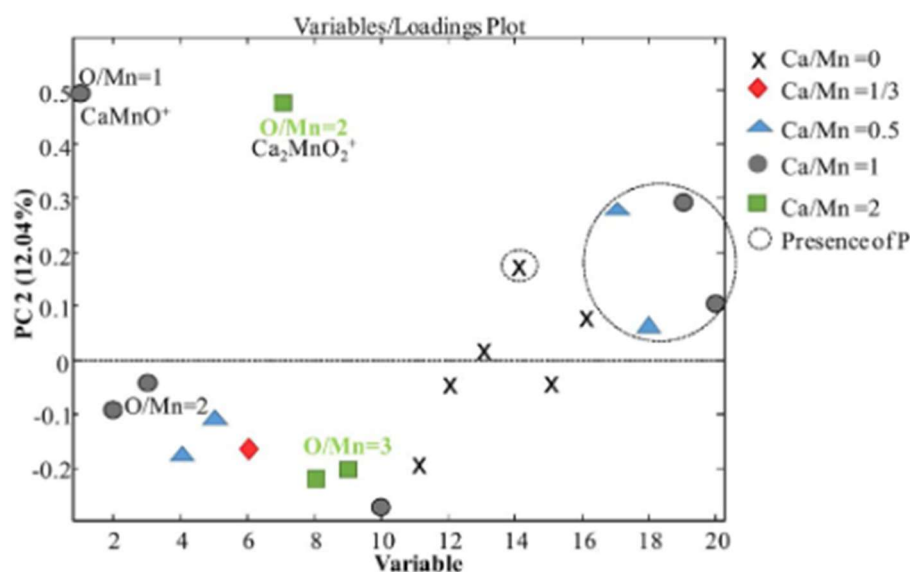


Fig. 9: Loading plot of PC2.

3.5. Discussion

The oxidation of toluene on hydroxyapatite supported manganese oxides is a complex reaction, as among other things, redox, oxygen mobility and acidity can play important roles in the reaction. Additionally, these parameters can be easily tuned by modifying the nature and number of active sites as well as metal-support interactions with change in manganese loading. It has been shown here that at low Mn loading (2.5 wt%) Mn^{2+} can be incorporated into the hydroxyapatite by substitution of Ca^{2+} . With increased Mn loadings (5-10 wt%) additional Mn can react with the surface to give well dispersed Mn oxide clusters taking advantages of OH groups at the surface of the hydroxyapatite. At higher Mn loadings (20-30 wt%) the detection by XRD of manganese oxide particles consistent with $\epsilon\text{-MnO}_2/\text{Mn}_2\text{O}_3$ phases is consistent with

a decrease in Mn dispersion. The global increase of the XPS Mn AOS with Mn content is in accordance with these different manganese locations. It is to be noted that the main PC (PC1) is able to discriminate the catalysts as a function of surface Mn dispersion as supported by **Fig.5b**. For low Mn loading the weak Mn(II)-O bond involved in the reaction can lead to the formation of more active oxygen species. Conversely assuming a Mars and Van Krevelen mechanism, Mn₂₀Hap and Mn₃₀Hap catalysts with highest Mn AOS would have highest oxidation activities. Soylu *et al.* [33] and Carabineiro *et al.* [34] have showed that the acidity of the catalyst has also to be taken account in toluene oxidation reaction. It was shown that toluene adsorption occurred through interaction of methyl and phenyl groups on catalyst surface followed by H and C subtraction [35-37]. Toluene has not to be strongly adsorbed (weak acid sites) in order to facilitate the subsequent oxygen attack from the lattice/surface of the catalyst. B.Chen *et al.* reported elsewhere [6] that the acidity of surface Hap increases when adding manganese suggesting that an intermediate acidity is required to better activate the toluene molecule. In this study, the Mn₅Hap catalyst appears to be the best catalyst for total oxidation of toluene. It might be composed of some Mn oxide clusters well-dispersed on Mn²⁺ incorporated hydroxyapatite taking advantage of a (Mn(II)/Mn(III)) valence pair, and might present a good oxygen mobility and an intermediate acidity. For higher Mn loading, the lower Mn dispersion precludes to get efficient catalysts whereas for lower Mn loading, a lower acidity might explain a lower activity.

The extent of deactivation has been shown to depend on the Mn local environment and location. The volcano plots obtained conjointly from the activity coefficient against Mn loading and from the PC2 score as a function of Mn content show that PC2 is clearly related to the deactivation extent of the catalysts. An investigation by ToF-SIMS in the 50-180 m/z range has been performed both in negative and positive polarities in order to track a possible chemical deactivation over the catalysts. The search of increase in intensity of possible organic fragment secondary ions originated from species formed through partial decomposition/oxidation of toluene and inorganic/organic secondary ions consistent with poisoning effects has been carried out. The possible change in intensity of the m/z = 60 signal relative to CO₃²⁻ has also been investigated to provide evidence of strongly bounded carboxylates. All these studies do not lead to significant differences in the intensity of the m/z signals when comparing the fresh and used catalysts discarding *a priori* such chemical schemes of deactivation. Furthermore it is difficult to ascertain some significant decrease of the mean crystallite size of the Mn₂O₃/ε-MnO₂ phases detected over Mn_xHap (x = 20 and 30) enabling to show a possible sintering of the Mn active phase. By opposition the decrease in toluene activity which occurs in the five first hours of the tests of stability could be attributed to a competition of the reactants and water for the specific sites as previously noticed by C. Lahousse *et al.* on γ-MnO₂ in the total oxidation of hexane [38]. Consistent with the PC2 loadings it is postulated a re-dispersion at the outermost layers of hydroxyapatite affecting the Ca-O-Mn interaction. This re-dispersion which mainly affects Mn₅Hap and Mn₁₀Hap samples might lead to a better resistance of the catalyst towards deactivation.

Conclusion

Synthesis of Hap supported MnOx materials (Mn wt%: 2.5, 5, 10, 20 and 30) has been carried out by wet impregnation using manganese (II) nitrate as precursor followed by calcination at 400 °C. It has been shown by XPS that Mn loading significantly affects the nature of manganese species in terms of Mn dispersion and average oxidation state. PCA assisted ToF-SIMS study allows to discriminate the catalysts by their surface manganese content (PC1) and behavior to deactivation (PC2) in relation through changes in Mn-O-Ca interactions.

Acknowledgements

Chevreul Institute (FR 2638), Ministère de l'Enseignement Supérieur et de la Recherche, Région Nord – Pas de Calais and FEDER are acknowledged for supporting and funding this work. D. Chlala acknowledges the award of a doctoral fellowship by the Agence Universitaire de la Francophonie (AUF) – Région du Moyen-Orient. M. Labaki is also very grateful to this institution for research fellowship. This work was also supported by a grant from the project PHC CEDRE 2015 N° 32933QE and by a grant from the Lebanese CNRS project N°01-08-15. The authors are grateful to Martine Trentesaux for XPS measurements.

References

- [1] H. Fernandez-Moran, A. Engström, *Nature* 178 (1956) 494.
- [2] J. Baton, A.J. Kadaksham, A. Nzihou, P. Singh, N. Aubry, *J. Hazard. Mater.* A139 (2007) 461.
- [3] A. Mortimer, J. Lemaitre, *J. Solid State Chem.* 78 (1989) 215.
- [4] S. Baillez, A. Nzihou, D. Bernache-Assolant, E. Champion, P. Sharrock, *J. Hazard. Mater.* 139 (2007) 443.
- [5] M. Hadioui, P. Sharrock, M.O. Mecherri, V. Brumas, M. Fiallo, *Chem. Pap.* 62 (2008) 516.
- [6] B. Chen, J. Li, W. Dai, L. Wang, S. Gao, *Green Chem.* 16 (2014) 3328.
- [7] Z. Qu, Y. Sun, D. Chen, Y. Wang, *J. Mol. Catal. A Chem.* 393 (2014) 182.
- [8] D. Chlala, J.-M. Giraudon, N. Nuns, C. Lancelot, R.-N. Vannier, M. Labaki, J.-F. Lamonier, *Appl. Catal. B: Environ.* 184 (2016) 84.
- [9] D. J. Graham, M.S. Wagner, D.G. Castner, *Appl. Surf. Sc.* 252 (2006) 6860.
- [10] F. Bertinchamps, C. Poleunis, C. Gregoire, P. Eloy, P. Bertrand, E. M. Gaigneaux, *Surf. Interface Anal.* 40 (2008) 231-238.
- [11] N. Nuns, A. Beaurain, D. Nguyen, A. Vandenbroucke, N. de Geyter, R. Morent, C. Leys, J.-M. Giraudon, J.-F. Lamonier, *Appl. Surf. Sci.* 320 (2014) 154-160.
- [12] A.M.C. Davies, *Spectroscopy Europe* 17 (2005) 30.
- [13] K.R. Beebe, B.R. Kowalski, *Anal. Chem.* 59 (1987) 1007A.
- [14] S.D. Brown, *Appl. Spectrosc.* 49 (1995) 14A.
- [15] E.V. Thomas, *Anal. Chem.* 66 (1994) 795A.
- [16] X.V. Eynde, P. Bertrand, *Surf. Interface. Anal.* 25 (1997) 878.
- [17] M.S. Wagner, D.G. Castner, *Langmuir* 17 (2001) 4649.
- [18] R. Canteri, G. Speranza, M. Anderle, S. Turri, S. Radice, *Surf. Inter. Anal.* 35 (2003) 318.
- [19] M.L. Pacholski, *Appl. Surf. Sci.* 231 (2004) 235.
- [20] H.B. Lu, C.T. Campbell, D.J. Graham, B.D. Ratner, *Anal. Chem.* 72 (2000) 2886.
- [21] F.M. Piras, M.F. Dettori, A. Magnani, *Appl. Surf. Sci.* 255 (2009) 7805.
- [22] M. Tagliabue, F. Bazzano, G. Del Piero, N. Panariti, C. Perego, *Catal. Today* 137 (2008) 119.

- [23] N. Pasadakis, C. Yiokari, N. Varotsis, C. Vayenas, *Appl. Catal. A: Gen.* 207 (2001) 333.
- [24] J.E. Hensley, S. Pylypenko, D. A. Ruddy, *J. Catal.* 309 (2014) 199.
- [25] Q. Wang, Y. Peng, J. Fu, G. Z. Kyzas, S.M. R. Billah, *S. An, Appl. Catal. B: Environ.* 168 (2001) 333.
- [26] A. Henrion, H. Ewald, H. Miessner, *Appl. Catal.* 62 (1990) 23.
- [27] X.Weng, B. Perston, X.Z. Wang, I. Abrahams, T. Lin, S. Yang, J. R.G. Evans, D.J. Morgan, A. F. Carley, M. Bowker, J. C. Knowles, I. Rehman, J.A. Darr, *Appl. Catal. B: Environ.* 90 (2009) 405.
- [28] C. A. Nunes, M. C. Guerreiro, *J. Mol. Cat. A: Chem.* 370 (2013) 145.
- [29] J. J. Spivey, G. W. Roberts and B. H. Davis (Eds.), *Catalyst Deactivation 2001, Studies in Surface Science and Catalysis*, 139 (2001) 290.
- [30] V.R. Galakhov, M. Demeter, S. Bartkowski, M. Neumann, N.A. Ovechkina, E.Z. Kurmaev, N.I. Lobachevskaya, Ya.M. Mukovskii, J. Mitchell, D.L. Ederer, *Phys. Rev. B* 65 (2002) 113102.
- [31] L. Silvester, J.-F. Lamonier, R.-N. Vannier, C. Lamonier, M. Capron, A.-S. Mamede, F. Pourpoint, A. Gervasini, F. Dumeignil, *J. Mater. Chem. A* 2 (2014) 11073.
- [32] W. Pon-On, S. Meejoo, I.-M. Tang, *Mater.Res.Bull.* 43 (2008) 2137.
- [33] G.S.P. Soylu, Z. Özcelik, I. Boz, *Chem. Eng. J.* 162 (2010) 380.
- [34] S.A.C. Carabineiro, X. Chen, M. Konsolakis, A.C. Psarras, P.B. Tavares, J.J.M. Órfão, M.F.R. Pereira, J.L. Figueiredo, *Catal. Today* 244 (2015) 161
- [35] E. Finocchio, G. Busca, V. Lorenzelli, R. J. Willey, *J. Catal.* 151 (1995) 204.
- [36] B. Irigoyen, A. Juan, S. Larrondo, N. Amadeo, *Surf. Sci.* 523 (2003) 252.
- [37] X. Tang, Y. Xu, W. Shen, *Chem. Eng. J.* 144 (2008) 175.
- [38] C. Lahousse, A. Bernier, P. Grange, B. Delmon, P. Papaefthimiou, T. Ioannides, and X. Verykios, *J. Catal.* 178 (1998) 214.